

Non-Kitaev spin liquids in Kitaev materials

Yao-Dong Li^{1,2}, Xu Yang^{3,6}, Yi Zhou^{4,5}, and Gang Chen^{1,6*}

¹*State Key Laboratory of Surface Physics and Department of Physics, Fudan University, Shanghai 200433, China*

²*Department of Physics, University of California Santa Barbara, CA 93106, United States*

³*Department of Physics, Boston College, Chestnut Hill, Massachusetts 02467, United States*

⁴*Beijing National Laboratory for Condensed Matter Physics,
and Institute of Physics, Chinese Academy of Sciences, Beijing 100190, China*

⁵*CAS Center for Excellence in Topological Quantum Computation,
University of Chinese Academy of Sciences, Beijing 100190, China and*

⁶*Department of Physics and Center of Theoretical and Computational Physics,
The University of Hong Kong, Pokfulam Road, Hong Kong, China*

(Dated: August 22, 2022)

We point out that the Kitaev materials may not necessarily support Kitaev spin liquid. It is well-known that having a Kitaev term in the spin interaction is not the sufficient condition for the Kitaev spin liquid ground state. Many other spin liquids may be stabilized by the competing spin interactions of the systems. We thus explore the possibilities of non-Kitaev spin liquids in the honeycomb Kitaev materials. We carry out a systematic classification of gapped \mathbb{Z}_2 spin liquids using the Schwinger boson representation for the spin variables. The presence of strong spin-orbit coupling in the Kitaev materials brings new ingredients into the projective symmetry group classification of the non-Kitaev spin liquid. We predict the spectroscopic properties of these gapped non-Kitaev spin liquids. Moreover, among the gapped spin liquids that we discover, we identify the spin liquid whose spinon condensation leads to the magnetic Bragg peak structure of the zig-zag magnetic order that was observed in Na_2IrO_3 and $\alpha\text{-RuCl}_3$. We further discuss the possibility of gapped \mathbb{Z}_2 spin liquid in pressurized $\alpha\text{-RuCl}_3$.

I. INTRODUCTION

Kitaev spin liquid was proposed by A. Kitaev when he constructed an elegant model and solved it exactly¹. An interesting connection to Na_2IrO_3 was made by G. Jackeli and G. Khaliulin². It was shown that the strong spin-orbit coupling (SOC) of iridium electrons could give rise to a Kitaev interaction in the effective spin Hamiltonian for the $j = 1/2$ iridium local moments. Since then, many iridates were synthesized and explored^{3–12}, including the recent $\alpha\text{-RuCl}_3$ ^{13–18} and the very early hyperkagome lattice spin liquid material $\text{Na}_4\text{Ir}_3\text{O}_8$ ¹⁹ where the $j = 1/2$ local moment^{20,21} and the anisotropic spin interaction were proposed²¹. These materials are dubbed “Kitaev materials” and have sparked an active search of Kitaev spin liquid^{22–26}.

Generally speaking, the list of Kitaev materials goes beyond iridates and ruthenates^{27–29}. What gives the Kitaev interaction is the strong SOC, and this is common to magnetic materials with heavy atoms. Therefore, any strong spin-orbit-coupled Mott insulator with spin-orbit-entangled effective spin-1/2 moments and a proper lattice geometry can be a Kitaev material. In particular, the rare-earth magnets, that have the same lattice structure as iridates and ruthenates, could be ideal Kitaev materials²⁷. Despite the growing list of Kitaev materials, all these systems face one crucial issue—there are many competing interactions that coexist with the Kitaev interaction. For example, for the nearest-neighbor bonds in Na_2IrO_3 and $\alpha\text{-RuCl}_3$, three extra interactions beyond the Kitaev interaction are present³⁰, not to mention many further neighbor (anisotropic) spin interactions that arise from the large spatial extension of the

$4d/5d$ electron wavefunction.

In fact it has been shown that Kitaev spin liquid is fragile and small perturbation could actually destabilize it^{31–35}. Meanwhile, the real materials contain many competing interactions that may be as important as the Kitaev interaction, the candidate quantum spin liquids (QSLs) for these materials remain to be examined. On the other hand, for any other gapped QSL that is not Kitaev spin liquid, if it is realized, it will be stable against small local perturbations regardless of the Kitaev interaction. This means that having the Kitaev interaction in the Hamiltonian is insufficient to induce Kitaev spin liquid and other competing interactions could instead favor different QSL ground states. For example, the J_1 - J_2 spin-1/2 Heisenberg model on the honeycomb lattice in certain parameter regime was proposed to support a gapped QSL that is clearly not a Kitaev spin liquid³⁶.

In this work, we deviate from the “hot spot” of searching for Kitaev spin liquid in Kitaev materials. Instead, our goal here is to find possible candidate QSLs in Kitaev materials that are not Kitaev spin liquid and to predict the experimental consequences of them. Considering the richness of Kitaev materials, it is very likely that these non-Kitaev QSLs may actually be stabilized in certain systems. A recent study of pressurized $\alpha\text{-RuCl}_3$ indeed suggested some evidence for a possible QSL³⁷. This experimental work motivates us to search for non-Kitaev QSLs in these systems. We carry out a systematic projective symmetry group (PSG) classification of gapped \mathbb{Z}_2 QSLs on a honeycomb lattice using Schwinger boson^{38–42} representation of the spins. Due to the spin-orbit-entangled nature of the local moments, the symmetry transformation operates both on the spin compo-

nents and on the spin position^{43–45}. This new symmetry property gives a different classification scheme from the existing PSG analysis. From the PSG results, we predict the spectroscopic properties of different \mathbb{Z}_2 QSLs on the honeycomb lattice. Moreover, we study the proximate magnetic orders out of the QSLs by condensing the spinons^{38,46}. The magnetic wavevector of the zig-zag magnetic order, that was observed in Na_2IrO_3 and $\alpha\text{-RuCl}_3$ ^{7,32,47}, naturally connects with the \mathbb{Z}_2 QSLs via the spinon condensation.

The remaining parts of the paper are organized as follows. In Sec. II, we introduce the Schwinger boson construction for the \mathbb{Z}_2 QSLs with spin-orbit-entangled local moments. In Sec. III, we explain the specific properties of the symmetry operations under the Schwinger boson framework. In Sec. IV, we obtain 16 distinct \mathbb{Z}_2 QSLs from the PSG classifications and study the phase diagram of several representative mean-field QSL states. In Sec. V, we explore the spectroscopic properties and the proximate magnetic phases of the aforementioned mean-field \mathbb{Z}_2 QSLs. Finally in Sec. VI, we discuss the relevant experiments and especially explain the possibilities for the pressurized $\alpha\text{-RuCl}_3$.

II. SCHWINGER BOSON CONSTRUCTION

The gapped \mathbb{Z}_2 spin liquids can be studied by either Schwinger boson or Abrikosov fermion approach. We here adopt the Schwinger boson construction since it is easier to explore the proximate magnetic orders with bosonic variables. In the Schwinger boson representation, the effective spin \mathbf{S}_i on site i is given by $\mathbf{S}_i = \frac{1}{2}b_{i\alpha}^\dagger \boldsymbol{\sigma}_{\alpha\beta} b_{i\beta}$ where $b_{i\alpha}$ ($\alpha = \uparrow, \downarrow$) is the bosonic spinon operator. The Hilbert space is enlarged due to the introduction of the spinons; to project out unphysical states, the constraint $\sum_\alpha b_{i\alpha}^\dagger b_{i\alpha} = 1$ on local boson number is imposed. The most general candidate mean-field Hamiltonian for the \mathbb{Z}_2 spin liquids has the following form,

$$H_{\text{MF}} = \sum_{\langle ij \rangle, \alpha\beta} (u_{ij, \alpha\beta}^A b_{i\alpha}^\dagger b_{j\beta} + u_{ij, \alpha\beta}^B b_{i\alpha} b_{j\beta} + h.c.) + \sum_i \mu_i (\sum_\alpha b_{i\alpha}^\dagger b_{i\alpha} - 1) \quad (1)$$

where we have restricted the mean-field ansatz to nearest neighbors and introduced the chemical potential μ_i to enforce the boson number constraint and we have used the superscript A/B to represent hopping/pairing terms in the coefficients u . Due to the spin-orbit-entangled nature of the local moments, the $\text{SU}(2)$ symmetry breaking terms exist in the mean-field ansatz. Using the hermiticity of the Hamiltonian and bosonic statistics of the spinons, it is easy to show that $u_{ij, \uparrow\downarrow}^B = u_{ji, \downarrow\uparrow}^B$, $u_{ij, \alpha\alpha}^B = u_{ji, \alpha\alpha}^B$, $u_{ij, \alpha\alpha}^A = (u_{ji, \alpha\alpha}^A)^*$, and $u_{ij, \uparrow\downarrow}^A = (u_{ji, \downarrow\uparrow}^A)^*$.

III. PROJECTIVE SYMMETRY GROUP

In this section we follow the projective symmetry group (PSG) approach introduced in Refs. 39 and 40 to classify the spinon mean field states based on the symmetries of the honeycomb layers of Kitaev materials. The spinon mean field state will be a reasonable description of the QSLs, provided the QSL survives the quantum fluctuations beyond mean field.

The lattice system of the honeycomb layer is shown in Fig. 1 and defined in Appendix A. The space group is generated by two translations T_1 and T_2 , a counter-clockwise sixfold rotation C_6 around the hexagon center, and a reflection σ around the horizontal axis through the same hexagon center. Under the symmetry operation \mathcal{O} , the bosonic spinon transforms as

$$b_i \rightarrow \hat{\mathcal{O}}^\dagger b_i \hat{\mathcal{O}} = \mathcal{G}_{\mathcal{O}(i)}^\mathcal{O} \mathcal{U}_\mathcal{O} b_{\mathcal{O}(i)} \quad (2)$$

where $\mathcal{G}_{\mathcal{O}(i)}^\mathcal{O} = e^{i\phi_{\mathcal{O}}[\mathcal{O}(i)]}$ is a local $\text{U}(1)$ gauge transformation, which leaves the spin operators invariant. The gauge transformation is generally nontrivial, hence incorporated in the symmetry operation in Eq. (2). After projection into the physical Hilbert space, spinons states related by a pure gauge transformation should give the same physical state. In Eq. (2) we have introduced the spin rotation $\mathcal{U}_\mathcal{O}$ to account for the effects of SOC, which rotates the position and spin simultaneously. In explicit forms, we have $\mathcal{U}_{T_1} = \mathcal{U}_{T_2} = \mathbf{1}_{2 \times 2}$, $\mathcal{U}_{C_6} = \exp(i\frac{\pi}{3}\frac{\sigma_z}{2})$, $\mathcal{U}_\sigma = \exp(i\pi\frac{\sigma_x}{2})$.

For mean-field Hamiltonian of the form in Eq. (1) to be invariant under the symmetry transformation \mathcal{O} , the coefficients should satisfy

$$u_{\mathcal{O}(i)\mathcal{O}(j), \alpha\beta}^A = (\mathcal{G}_{\mathcal{O}(i)}^\mathcal{O})^* \mathcal{G}_{\mathcal{O}(j)}^\mathcal{O} (\mathcal{U}_\mathcal{O}^*)_{\alpha\nu} (\mathcal{U}_\mathcal{O})_{\beta\lambda} u_{ij, \nu\lambda}^A, \quad (3)$$

$$u_{\mathcal{O}(i)\mathcal{O}(j), \alpha\beta}^B = \mathcal{G}_{\mathcal{O}(i)}^\mathcal{O} \mathcal{G}_{\mathcal{O}(j)}^\mathcal{O} (\mathcal{U}_\mathcal{O})_{\alpha\nu} (\mathcal{U}_\mathcal{O})_{\beta\lambda} u_{ij, \nu\lambda}^B, \quad (4)$$

where we have used the fact that $\mathcal{U}_\mathcal{O}$ commutes with $\mathcal{G}^\mathcal{O}$. For a general pair of sites (i, j) , the above equations are solvable if for each group relation $\mathcal{O}_1 \mathcal{O}_2 \cdots \mathcal{O}_n = 1$, the

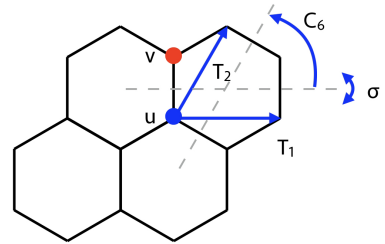


FIG. 1. The honeycomb lattice and its symmetries. Blue/red circles indicate the two sublattices denoted as u/v . The space-group generators are translations T_1 and T_2 , sixfold rotation C_6 around the plaquette center, and horizontal reflection σ through the hexagon center.

\mathbb{Z}_2 QSL	\mathcal{G}^{T_1}	\mathcal{G}^{T_2}	\mathcal{G}^{C_6}	$\mathcal{G}^\sigma[u]$	$\mathcal{G}^\sigma[v]$
$\mathbb{Z}_2\text{A000}$	1	1	1	1	1
$\mathbb{Z}_2\text{A001}$	1	1	i	i	$-i$
$\mathbb{Z}_2\text{A010}$	1	1	i	1	1
$\mathbb{Z}_2\text{A011}$	1	1	-1	i	$-i$
$\mathbb{Z}_2\text{A100}$	1	1	i	i	i
$\mathbb{Z}_2\text{A101}$	1	1	-1	-1	1
$\mathbb{Z}_2\text{A110}$	1	1	-1	i	i
$\mathbb{Z}_2\text{A111}$	1	1	$-i$	-1	1
$\mathbb{Z}_2\text{B000}$	1	$(-1)^x$	$i^{x(x+2y-1)}$	$i^{2x+y(y+1)}$	$i^{2x+y(y+1)}$
$\mathbb{Z}_2\text{B001}$	1	$(-1)^x$	$i^{x(x+2y-1)+1}$	$i^{2x+y(y+1)+1}$	$i^{2x+y(y+1)-1}$
$\mathbb{Z}_2\text{B010}$	1	$(-1)^x$	$i^{x(x+2y-1)+1}$	$i^{2x+y(y+1)}$	$i^{2x+y(y+1)}$
$\mathbb{Z}_2\text{B011}$	1	$(-1)^x$	$i^{x(x+2y-1)+2}$	$i^{2x+y(y+1)+1}$	$i^{2x+y(y+1)-1}$
$\mathbb{Z}_2\text{B100}$	1	$(-1)^x$	$i^{x(x+2y-1)+1}$	$i^{2x+y(y+1)+1}$	$i^{2x+y(y+1)+1}$
$\mathbb{Z}_2\text{B101}$	1	$(-1)^x$	$i^{x(x+2y-1)+2}$	$i^{2x+y(y+1)+2}$	$i^{2x+y(y+1)}$
$\mathbb{Z}_2\text{B110}$	1	$(-1)^x$	$i^{x(x+2y-1)+2}$	$i^{2x+y(y+1)+1}$	$i^{2x+y(y+1)+1}$
$\mathbb{Z}_2\text{B111}$	1	$(-1)^x$	$i^{x(x+2y-1)+3}$	$i^{2x+y(y+1)+2}$	$i^{2x+y(y+1)}$

TABLE I. List of the gauge transformations associated with the symmetry operations of the 16 \mathbb{Z}_2 QSLs, where (x, y, w) denotes the site in the honeycomb coordinate system.

following identities are satisfied,

$$\mathcal{U}_{\mathcal{O}_1}\mathcal{U}_{\mathcal{O}_2}\cdots\mathcal{U}_{\mathcal{O}_n}\mathcal{G}_i^{\mathcal{O}_1}\mathcal{G}_{\mathcal{O}_2\mathcal{O}_3\cdots\mathcal{O}_n(i)}^{\mathcal{O}_2}\mathcal{G}_{\mathcal{O}_3\cdots\mathcal{O}_n(i)}^{\mathcal{O}_3}\cdots\mathcal{G}_{\mathcal{O}_n(i)}^{\mathcal{O}_n}=\pm 1$$

$$\Leftrightarrow \mathcal{G}_i^{\mathcal{O}_1}\mathcal{G}_{\mathcal{O}_2\mathcal{O}_3\cdots\mathcal{O}_n(i)}^{\mathcal{O}_2}\mathcal{G}_{\mathcal{O}_3\cdots\mathcal{O}_n(i)}^{\mathcal{O}_3}\cdots\mathcal{G}_{\mathcal{O}_n(i)}^{\mathcal{O}_n}=\pm 1, \quad (5)$$

where ± 1 is either element of \mathbb{Z}_2 , the invariant gauge group (IGG). The IGG turns out to be the gauge group of the low-energy effective theory of the QSL state^{39,40}. Here, since we are considering \mathbb{Z}_2 QSLs, the IGG should also be \mathbb{Z}_2 . The two lines in Eq. (5) are equivalent because the identity element involves either rotation by 0 or 2π , so $\mathcal{U}_{\mathcal{O}_1}\mathcal{U}_{\mathcal{O}_2}\cdots\mathcal{U}_{\mathcal{O}_n}=\pm 1$, and the group relations constraint only the phases $\phi_{\mathcal{O}}$. Given the defining relations between group generators T_1, T_2, C_6, σ , we can solve for all the possible gauge transformation functions $\phi_{\mathcal{O}}(i)$'s compatible with Eq. (5).

IV. THE 16 CLASSES OF \mathbb{Z}_2 QSLS AND THE MEAN-FIELD PHASE DIAGRAM

The solutions of the $\phi_{\mathcal{O}}$'s for equations of the form in Eq. (5) are as follows:

$$\phi_{T_1}(x, y, w) = 0, \quad (6)$$

$$\phi_{T_2}(x, y, w) = p_1\pi x, \quad (7)$$

$$\phi_{C_6}(x, y, w) = \frac{\pi}{2}(p_1x(x+2y-1)+p_7+p_8+p_9), \quad (8)$$

$$\phi_{\sigma}(x, y, u) = \frac{\pi}{2}(2p_1x+p_1y(y+1)+p_7+p_9), \quad (9)$$

$$\phi_{\sigma}(x, y, v) = \frac{\pi}{2}(2p_1x+p_1y(y+1)+p_7-p_9). \quad (10)$$

where $w = u, v$ and p_1, p_7, p_8, p_9 are free to take either 0 or 1 in \mathbb{Z}_2 . Details of the derivation can be found in

\mathbb{Z}_2 QSL	u_s^A	u_a^A	u_s^B	u_a^B
$\mathbb{Z}_2\text{A000}$	$\neq 0$	$\neq 0$	0	0
$\mathbb{Z}_2\text{A001}$	0	$\neq 0$	$\neq 0$	0
$\mathbb{Z}_2\text{A010}$	$\neq 0$	$\neq 0$	$\neq 0$	0
$\mathbb{Z}_2\text{A011}$	0	$\neq 0$	0	0
$\mathbb{Z}_2\text{A100}$	$\neq 0$	$\neq 0$	$\neq 0$	$\neq 0$
$\mathbb{Z}_2\text{A101}$	0	$\neq 0$	0	$\neq 0$
$\mathbb{Z}_2\text{A110}$	$\neq 0$	$\neq 0$	0	$\neq 0$
$\mathbb{Z}_2\text{A111}$	0	$\neq 0$	$\neq 0$	$\neq 0$
$\mathbb{Z}_2\text{B000}$	$\neq 0$	$\neq 0$	0	0
$\mathbb{Z}_2\text{B001}$	0	$\neq 0$	$\neq 0$	0
$\mathbb{Z}_2\text{B010}$	$\neq 0$	$\neq 0$	$\neq 0$	0
$\mathbb{Z}_2\text{B011}$	0	$\neq 0$	0	0
$\mathbb{Z}_2\text{B100}$	$\neq 0$	$\neq 0$	$\neq 0$	$\neq 0$
$\mathbb{Z}_2\text{B101}$	0	$\neq 0$	0	$\neq 0$
$\mathbb{Z}_2\text{B110}$	$\neq 0$	$\neq 0$	0	$\neq 0$
$\mathbb{Z}_2\text{B111}$	0	$\neq 0$	$\neq 0$	$\neq 0$

TABLE II. A simplified list of coefficients in the mean-field Hamiltonians of each class of \mathbb{Z}_2 QSLs. In the list, $u_{s/a}^A$ stands for coefficients for spin-preserving/spin-flipping spinon hopping terms, and $u_{s/a}^B$ stands for coefficients for spin-preserving/spin-flipping spinon pairing terms. The list emphasizes the vanishing parameters; for a complete list, see Tab. III.

Appendix B. Therefore there are in total 16 states labeled by p_1, p_7, p_8 and p_9 . Specifically, the state is called $\mathbb{Z}_2\text{Ap}_7p_8p_9$ states when $p_1 = 0$, and $\mathbb{Z}_2\text{Bp}_7p_8p_9$ states when $p_1 = 1$. This p_1 variable is proportional to the magnetic flux $p_1\pi$ through each unit cell felt by the spinon. It signifies the fractionalization of translation symmetry to be discussed in Sec. V.

With the PSG solutions in Tab. I, we obtain the mean-field Hamiltonians for Schwinger bosons in Appendix C. The simplified results are summarized in Tab. II. Due to constraints from the PSG, the hermiticity of the Hamiltonian, and time-reversal symmetry, some of the coefficients are fixed to be 0.

The classification of \mathbb{Z}_2 QSLs incorporate a wide range of phases (at least one for each class) and encode different types of interactions. This is particularly relevant to Kitaev materials, where interactions beyond the Kitaev model compete with the Kitaev term. These interactions can drive the system away from the Kitaev spin liquid state into other \mathbb{Z}_2 QSLs, or even destabilize the spin liquid and introduce a magnetic order. It is therefore desirable to investigate the phase diagram for the \mathbb{Z}_2 QSL states in our classification and determine the ranges of the parameters that support a QSL phase. We can further predict their proximate magnetic orders that can be directly compared with experiments.

The magnetic order out of the \mathbb{Z}_2 QSLs can be understood in the following manner. In the \mathbb{Z}_2 QSL phases, the spinons are fully gapped, and the system are absent from developing long-range order. However, as we have

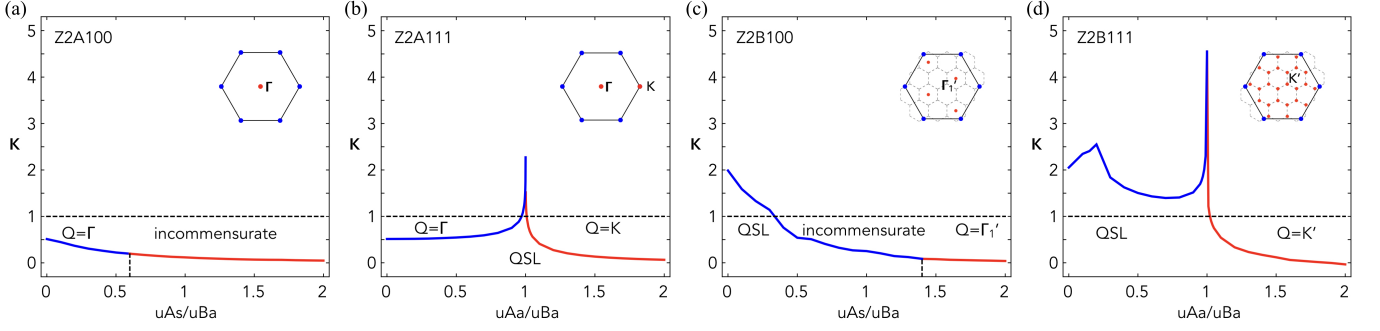


FIG. 2. The phase diagrams for representative mean-field Hamiltonians. Here κ is the average boson density, defined to be $\sum_{i,\alpha} \langle b_{i\alpha}^\dagger b_{i\alpha} \rangle / N_{\text{site}}$, and \mathbf{Q} is the position in Brillouin zone of the spinon band minimum. In (a) and (c), we choose $u_a^A/u_s^A = 0.6$ and $u_s^B = 0$, and in (b) and (d) we choose $u_s^B = 0$. The solid line marks the phase boundary between magnetic ordered state (above solid line) and the \mathbb{Z}_2 QSL states (below solid line). Here we use different colors for solid lines to indicate different ordered states above the solid lines. The choice of the momenta can be found in Appendix A.

mentioned in Sec. II, the spinon density must satisfy the uniform filling condition

$$\kappa = \langle b_{i\alpha}^\dagger b_{i\alpha} \rangle = 1. \quad (11)$$

Such a constraint is met by tuning the chemical potential μ within the mean field theory. At a critical value of μ , the spinon gap will close and the spinons condense at the band minimum \mathbf{Q} with $\langle b_{\mathbf{Q}\alpha} \rangle \neq 0$. It will correspondingly give rise to a magnetic order or spin density wave with ordering wavevector $2\mathbf{Q}$ (see Sec. VB).

Here we choose four representative classes, Z2A100, Z2A111, Z2B100, Z2B111, and solve for their mean-field phase diagrams (see Fig. 2). We found that the Z2A111, Z2B100, Z2B111 states all support paramagnetic QSL phases in the chosen parameter regime, and all of these QSL states can be driven to magnetic order when certain parameters are tuned.

V. EXPERIMENTAL CONSEQUENCES OF \mathbb{Z}_2 QSLs

In this section we discuss two experimental consequences of the \mathbb{Z}_2 QSLs. First, we note that translation symmetry fractionalization in Z2B states will result in an enhanced periodicity of the lower edge of the dynamic spin structure factor, which serves as a direct spectroscopic probe for the QSLs. Second, we study magnetic ordered states adjacent to QSLs via the condensation of Schwinger bosons. It turns out that the ordering nature of the boson-condensed state are determined by the classes of QSLs. Therefore the experimentally measured magnetic ordered states will impose restrictions on possible adjacent \mathbb{Z}_2 QSLs, which helps determine the nature of the experimentally realized spin liquids.

A. Spectroscopic signatures of translational symmetry fractionalization

A unique feature of QSLs is the emergent fractionalized excitations; in our case, these are the gapped spinons or visons. The spinons carry quantum numbers that are fractions of a physical spin. This fact prevents spinons from being directly probed, since any local observable is necessarily with integer quantum number, and the observable necessarily adopts a “convoluted” form in terms of spinon variables. In inelastic neutron scattering experiments, one neutron flip event creates a spin-1 excitation, and the energy-transfer of the neutron is shared between a pair of spin-1/2 spinons,

$$\mathbf{q} = \mathbf{k}_1 + \mathbf{k}_2, \quad (12)$$

$$\Omega(\mathbf{q}) = \omega(\mathbf{k}_1) + \omega(\mathbf{k}_2). \quad (13)$$

In the previous section we classified gapped \mathbb{Z}_2 QSLs on the honeycomb lattice, each characterized by a projective representation the emergent spinons live in. It was realized that the symmetry class of spinons has dramatic effects on the neutron spectrum^{48,49}. For the lattice translation, the relevant quantum number is p_1 , and we find

$$\phi_{T_1}(x, y, w) = 0, \quad (14)$$

$$\phi_{T_2}(x, y, w) = p_1 \pi x. \quad (15)$$

For the Z2B states, $p_1 = 1$, and the PSG elements corresponding to T_1 and T_2 anticommute,

$$\hat{T}_1 \hat{T}_2 \hat{T}_1^{-1} \hat{T}_2^{-1} = -1. \quad (16)$$

where \hat{T}_1 and \hat{T}_2 act on the spinon degrees of freedom instead on the spins. As a consequence, the periodicity of the lower excitaiton edge of the dynamic spin structure factor defined by

$$\text{edge}(\mathbf{q}) = \min_{\mathbf{k}} [\omega(\mathbf{k}) + \omega(\mathbf{q} - \mathbf{k})] \quad (17)$$

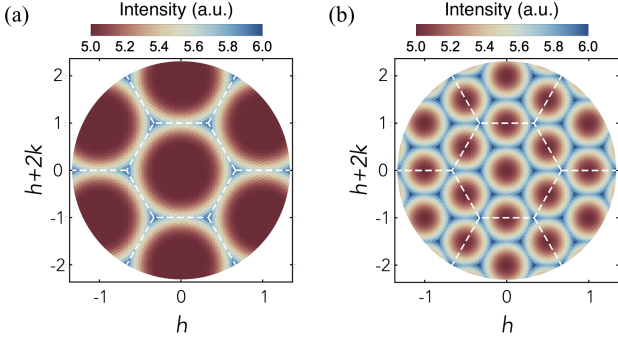


FIG. 3. (Color online.) Intensity plot of lower excitation edges of $\mathcal{S}(\mathbf{q}, \omega)$ for the (a) Z2A100 and (b) Z2B100 states. We have chosen $u_s^A = 2$, $u_a^A = 1.2$, $u_s^B = 0$, $u_a^B = 1$ (see Tab. II and Appendix B for definitions of the parameters). The white dashed lines mark the Brillouin zone boundary.

is doubled (see Appendix C),

For the Z2A states, the lower excitation edge should have the usual periodicity of 2π in both directions of Brillouin zone basis.

We illustrate the two possible fractionalization patterns in Fig. 3 representative Z2A and Z2B states. This pattern is accessible to neutron scattering experiments.

B. Proximate magnetic orders of \mathbb{Z}_2 QSLs

Besides the symmetry fractionalization in the QSL phases, the proximate magnetic orders in the spinon-condensed phases provide a complementary description of the system. Instead of two-spinon continuum, one expects to see sharp magnon peaks in the neutron or the resonant inelastic X-ray scattering data. Therefore, the enhanced spectral periodicity in the previous section is no longer a relevant description; it is much more feasible to directly probe the magnetic order. It would make a strong case for the \mathbb{Z}_2 QSL parent state if some of the magnetic orders depicted in Fig. 2 are observed.

In fact, we show here that the proximate magnetic order of the Z2B100 state (see Fig. 2c) has the same ordering wave vector $(\pi, 0)$ as the zig-zag order with ordering wave vector observed in Kitaev materials α -RuCl₃ and Na₂IrO₃.

The mean-field Hamiltonian Eq. (1) of a typical Z2B state in momentum space reads

$$H = \sum_{\mathbf{k} \in \frac{1}{2}\text{BZ}} \Psi_{\mathbf{k}}^\dagger (h(\mathbf{k}) - \mu) \Psi_{\mathbf{k}} \quad (18)$$

where

$$\Psi_{\mathbf{k}} = (b_{\mathbf{k},w,\alpha,m}, b_{-\mathbf{k},w,\alpha,m}^\dagger) \quad (19)$$

and $w = u, v$ labels the u and v sublattices of the honeycomb lattice, $\alpha = \uparrow, \downarrow$ labels the spin indices, and $m = 0, 1$

labels the sites in each magnetic unit cell (due to the π -flux in each of the original unit cell). The spectrum has an enhanced periodicity as expected.

As we see from Fig. 2c, in a large range of parameters the high symmetry points $\pm \mathbf{Q} = \Gamma'_1 = (\pm\pi/2, 0)$ are the two independent minimum of the spinon band structure in the magnetic Brillouin zone for the Z2B100 state. Moreover, the spinons condense at band minima in that regime, and the system is magnetically ordered. The corresponding spinon condensate has the following form:

$$\begin{aligned} & [\langle b_{\mathbf{r},u,\uparrow,0} \rangle, \langle b_{\mathbf{r},u,\uparrow,0}^\dagger \rangle, \dots, \langle b_{\mathbf{r},v,\downarrow,1} \rangle, \langle b_{\mathbf{r},v,\downarrow,1}^\dagger \rangle]^T \\ &= z_1^{\mathbf{Q}} \Psi_1^{\mathbf{Q}} e^{i\mathbf{Q} \cdot \mathbf{r}} + z_1^{-\mathbf{Q}} \Psi_1^{-\mathbf{Q}} e^{-i\mathbf{Q} \cdot \mathbf{r}} \\ &+ z_2^{\mathbf{Q}} \Psi_2^{\mathbf{Q}} e^{i\mathbf{Q} \cdot \mathbf{r}} + z_2^{-\mathbf{Q}} \Psi_2^{-\mathbf{Q}} e^{-i\mathbf{Q} \cdot \mathbf{r}}, \end{aligned} \quad (20)$$

where $\Psi_{1,2}^{\mathbf{Q}}$ and $\Psi_{1,2}^{-\mathbf{Q}}$ are eigenvectors of $h(\mathbf{k})$ at $\pm \mathbf{Q}$ with the lowest energy, respectively.

The choices of the coefficient z 's are subject to following constraints:

- 1) The condition $\langle b_{\mathbf{r},\alpha} \rangle^* = \langle b_{\mathbf{r},\alpha}^\dagger \rangle$ for all \mathbf{r} fixes $z_{1,2}^{-\mathbf{Q}}$ with respect to $z_{1,2}^{\mathbf{Q}}$;
- 2) The boson density $\langle n_{\mathbf{r}} \rangle = \sum_{\alpha} \langle b_{\mathbf{r},\alpha}^\dagger \rangle \langle b_{\mathbf{r},\alpha} \rangle$ should be uniform across the lattice system. This condition will fix $|z_1^{\mathbf{Q}}|^2 + |z_2^{\mathbf{Q}}|^2$.

With the condensate, it is ready to calculate the magnetic order with

$$\langle \mathbf{S}_{\mathbf{r}} \rangle = \frac{1}{2} \langle b_{\mathbf{r},\alpha}^\dagger \rangle \boldsymbol{\sigma}_{\alpha\beta} \langle b_{\mathbf{r},\beta} \rangle. \quad (21)$$

We see immediately that the magnetic order has an ordering wave vector of $2\mathbf{Q} = (\pi, 0)$, consistent with the experimentally observed magnetic Bragg peak, and the magnetic order is controlled by two real parameters while the overall phase factor is inessential. We have a limited set of free parameters for the magnetic order, so the magnetic order would take a rather fixed pattern, as illustrated in Fig. 4. As the zig-zag order, the ordering pattern is periodic in the chain direction and antiferromagnetic between the neighboring chains.

Although the order differs from the zig-zag or stripe ones, we suspect that this is an artifact of the spinon mean-field theory approach. In this framework, we are effectively dealing with a theory of free spinons with only nearest neighbor hopping. We expect that when further neighbor hoppings and interlayer interactions are taken into account, the magnetic order should be closer to reality. On the other hand, the π -flux is a robust feature and will survive interactions. Consequently, the $2\mathbf{Q}$ ordering wave vector will exist for a large range of parameters.

To further constrain the Z2B states with the Z2A states, we note that the proximate magnetic orders in the phase diagrams of Z2A states in Fig. 2 are either incommensurate with the lattice, or have an ordering vector of 2Γ or $2\mathbf{K}$. As a consequence, the resulting magnetic order is either ferromagnetic (see Appendix E) or an antiferromagnetic order. Both are drastically different from the zig-zag order that was observed.

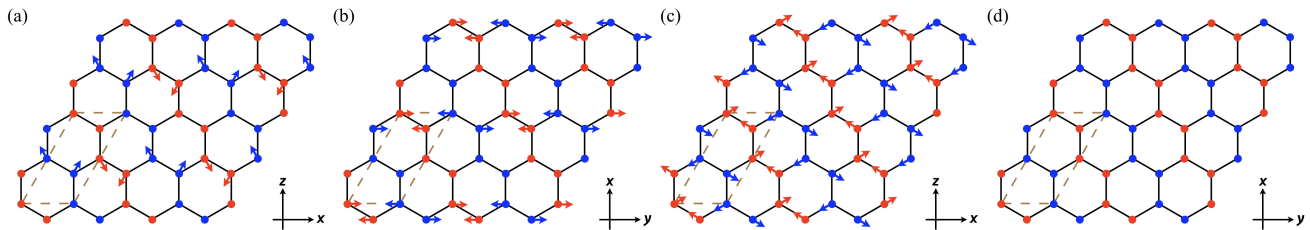


FIG. 4. (Color online.) The magnetic order for a $\mathbb{Z}_2\text{B100}$ state. We have split the components in x - z plane and along y -direction for clarity. Blue and red sites are the antiferromagnetically aligned chains along the direction perpendicular to $2\mathbf{Q}$. The gray dashed lines denote the enlarged unit cell. The parameters of the Hamiltonian are the same as in Fig. 3. In (a) and (b), we have chosen $|z_1^{\mathbf{Q}}| = |z_2^{\mathbf{Q}}|$, and $\arg z_2 - \arg z_1 = \pi/3$. In (c) and (d), we depict the order for $|z_2^{\mathbf{Q}}| = 0$. Notice that in the latter case the magnetic order is completely in the x - z plane.

In summary, we have pointed out that the $\mathbb{Z}_2\text{B100}$ state is likely to be the QSL state adjacent to the zig-zag ordered states observed in Kitaev materials $\alpha\text{-RuCl}_3$ and Na_2IrO_3 .

VI. DISCUSSION

The proposed *honeycomb* lattice Kitaev materials are Li_2IrO_3 , Na_2IrO_3 , and $\alpha\text{-RuCl}_3$ with $4d/5d$ magnetic ions. Unfortunately, all three materials develop long-range magnetic orders, and the relevant magnetic orders were proposed to be the zig-zag like with a magnetic unit cell that is twice of the crystal unit cell^{7,32,47}. For $\alpha\text{-RuCl}_3$ that is under an active study recently, the magnetic field is found to suppress the magnetism and possibly generate a QSL state at intermediate magnetic fields. The thermal Hall measurement has found a non-vanishing thermal Hall effect that seems to be consistent with the prediction from the chiral majorana fermion edge state that is obtained from the Kitaev spin liquid by the magnetic field^{50–52}. Because of the particular experimental setup in the thermal Hall measurements, Refs. 53 and 54 carefully considered the effect of the spin-lattice coupling and suggested that the quantization of the thermal Hall effect may survive and can actually be robust even with the spin-lattice coupling. These results may explain the thermal Hall effect in $\alpha\text{-RuCl}_3$. In contrast, our result in this paper is not dealing with the actual spin state in the intermediate magnetic fields. Instead, we are interested in the zero-field magnetic state and try to understand whether the magnetic orders can be thought as the proximate magnetic orders of the nearby \mathbb{Z}_2 QSLs. Thus, an indirect experimental signature would be a possible quantum phase transition from the current magnetic orders to the nearby \mathbb{Z}_2 QSLs. It is not obvious if this transition can be induced by the external magnetic field. It is, however, possible that the magnetic field induces the magnetic order from the \mathbb{Z}_2 QSLs via the spinon condensation where the magnetic field suppresses the spinon band gap.

On the other hand, a recent theoretical development⁵⁵ has extended the Schwinger boson construction to un-

derstand the dynamical properties of the magnetically ordered state that is obtained by condensing the bosonic spinons. Ref. 55 applies this theory to study the dynamical properties of the triangular lattice Heisenberg model, despite this model supports the well-known 120-degree magnetic order. Their results suggested that the Schwinger boson approach can be an adequate starting point for describing the excitation spectrum of some magnetically ordered compounds that are near the quantum melting point separating this ordered phase from the proximate QSL. In $\alpha\text{-RuCl}_3$, the ordered moment is only about 1/3 of the full magnetic moment in the paramagnetic phase¹⁸. Thus, it is natural and interesting to see whether Ref. 55's approach can be adapted to provide a new understanding of the spin dynamics inside the magnetic ordered state of $\alpha\text{-RuCl}_3$ rather than making connection to the Kitaev spin liquid.

The pressurized $\alpha\text{-RuCl}_3$ has been studied experimentally³⁷, as well as other strain effect experiments have been performed. We focus our discussion on the pressurized experiments³⁷. It is found that, above a critical pressure, the antiferromagnetic order in $\alpha\text{-RuCl}_3$ disappears and a possible QSL state appears. At even higher pressures, the system experiences a resistance drop by several orders in magnitude. This was interpreted as the softening or the closing of the charge gap. At the mean time, the magnetoresistivity in this range of pressure remain insensitive to the magnetic field up to 7T. There are several puzzles associated with this pressurized experiment. What is the nature of the disordered state when the magnetic order disappears? What is the nature of the disordered state with a significantly reduced resistance in the high pressure regime? What do the spin degrees of freedom do in this high pressure regime? The experimental information is quite limited to address these questions. However, here we would like make a bold suggestion. First, we propose that the disordered state can be a QSL state. The absence of the phase transition in the heat capacity measurement down to 4K suggests that the candidate QSL cannot be a symmetry broken state such as the time reversal symmetry broken chiral spin liquid. From the robustness of a phase in a large range of pressures, the candidate state may be a \mathbb{Z}_2 QSL, and

this \mathbb{Z}_2 topological order would survive even to the pressure when the charge gap is suppressed. In fact, Ref. 37 has attributed the insensitivity of the magnetoresistance to the magnetic field to the dominance of the spin energy scale. In the future experiments, it will be interesting to perform an inelastic neutron scattering measurement to check if the spinon continuum shows a spectral periodicity enhancement. In addition, doping the pressurized materials and examining the possibility of superconductivity or non-Fermi liquid behaviors can be quite interesting too. It is interesting to notice that doping the spin-orbit-coupled Mott insulators such as RuCl_3 , iridates, or any others with spin-orbit-entangled local moments beyond the $4d^5/5d^5$ $j = 1/2$ moments would necessarily experience an electron-hole doping asymmetry. This doping asymmetry arises from the distinct spin-orbital reconstruction/entanglement of the different electron occupation configurations from electron and hole doping. We will elaborate this general point in a later paper.

Quite recently, a theory work⁵⁶ by Zheng-Xin Liu and Bruce Normand considered the K - Γ model in magnetic fields and performed variational Monte Carlo calculations with Abrikosov fermion construction on the honeycomb lattice. They found both a gapless Dirac QSL and a Kalmeyer-Laughlin-type chiral QSL for different ranges and orientations of magnetic fields. More recently, a couple numerical and theoretical works^{57–59} suggested the field induced spinon Fermi surface QSL for the Kitaev model in magnetic fields. These QSLs in magnetic fields are also non-Kitaev QSLs,

To summarize, in this paper we have carefully classified the possible \mathbb{Z}_2 QSLs and studied the experimental signatures such as the proximate magnetic orders, symmetry fractionalization of the spinons, and the structure of the spinon continuum. Our results provide a rather different perspective from the existing thoughts on these Kitaev materials.

VII. ACKNOWLEDGMENTS

YDL and GC is supported by the Ministry of Science and Technology of China with Grant No. 2016YFA0301001, 2016YFA0300500, 2018YFGH000095. XY is supported from the National Science Foundation under Grant No.DMR-1151440. YZ is supported by National Key Research and Development Program of China (No.2016YFA0300202), National Natural Science Foundation of China (No.11774306), and the Strategic Priority Research Program of Chinese Academy of Sciences (No.XDB28000000).

Appendix A: The coordinate system and space group

The honeycomb lattice is illustrated in Fig. 1 of the main text. We choose the basis vectors to be

$$\mathbf{a}_1 = (1, 0), \quad \mathbf{a}_2 = \left(\frac{1}{2}, \frac{\sqrt{3}}{2}\right). \quad (\text{A1})$$

The lattice sites are labeled by (x, y, w) , where $w = u, v$ is the sublattice index. The position of the site (x, y, w) is

$$\mathbf{r}(x, y, w) = \begin{cases} x\mathbf{a}_1 + y\mathbf{a}_2, & \text{if } w = u, \\ x\mathbf{a}_1 + y\mathbf{a}_2 + \left(0, \frac{1}{\sqrt{3}}\right), & \text{if } w = v. \end{cases} \quad (\text{A2})$$

All momenta vectors are represented in the $\{\mathbf{v}_1, \mathbf{v}_2\}$ basis, where

$$\mathbf{v}_1 = \left(1, -\frac{1}{\sqrt{3}}\right), \quad \mathbf{v}_2 = \left(0, \frac{2}{\sqrt{3}}\right), \quad (\text{A3})$$

so that $\mathbf{a}_i \cdot \mathbf{v}_j = \delta_{ij}$. Therefore, the basis vectors of the Brillouin zone has the following forms,

$$\mathbf{b}_1 = (2\pi, 0), \quad \mathbf{b}_2 = (0, 2\pi), \quad (\text{A4})$$

and

$$\mathbf{\Gamma} = (0, 0), \quad (\text{A5})$$

$$\mathbf{M} = (\pi, 0) \text{ or } (0, \pi) \text{ or } (\pi, \pi) \quad (\text{A6})$$

$$\mathbf{K} = \left(\frac{4\pi}{3}, \frac{2\pi}{3}\right) \text{ or } \left(\frac{2\pi}{3}, \frac{4\pi}{3}\right). \quad (\text{A7})$$

We define additional high-symmetry points in the Brillouin zone,

$$\mathbf{\Gamma}' = \left(\frac{\pi}{2}, \frac{\pi}{2}\right) + a\left(\frac{2\pi}{3}, \frac{\pi}{3}\right) + b\left(\frac{\pi}{3}, \frac{2\pi}{3}\right), \quad (\text{A8})$$

where $a, b \in \mathbb{Z}$. $\mathbf{\Gamma}'_1$ corresponds to those with $a - b = 0 \pmod{3}$, and $\mathbf{\Gamma}'_2$ those with $a - b \neq 0 \pmod{3}$. Finally,

$$\mathbf{K}' = \mathbf{\Gamma}' + \left(0, \frac{\pi}{3}\right) \text{ or } \mathbf{K}' = \mathbf{\Gamma}' + \left(\frac{\pi}{3}, \frac{\pi}{3}\right). \quad (\text{A9})$$

The symmetry group of the honeycomb lattice consists of translations T_1, T_2 , a six-fold rotation C_6 and a reflection σ . Explicitly in terms of the lattice indices, their actions read

$$T_1 : (x, y, w) \rightarrow (x + 1, y, w), \quad w = u, v \quad (\text{A10})$$

$$T_2 : (x, y, w) \rightarrow (x, y + 1, w), \quad w = u, v \quad (\text{A11})$$

$$C_6 : \begin{cases} (x, y, u) \rightarrow (-y + 1, x + y - 1, v), \\ (x, y, v) \rightarrow (-y, x + y, u), \end{cases} \quad (\text{A12})$$

$$\sigma : \begin{cases} (x, y, u) \rightarrow (x + y, -y, v), \\ (x, y, v) \rightarrow (x + y, -y, u). \end{cases} \quad (\text{A13})$$

Appendix B: Algebraic solution of the \mathbb{Z}_2 PSG on honeycomb lattice

In this appendix we show classification of algebraic \mathbb{Z}_2 QSLs by solving the PSG defined in Sec. III.

The space group of the honeycomb lattice and its elements are defined in Sec. III. Presentations of the space group are

$$\begin{aligned} T_1^{-1}T_2T_1T_2^{-1} &= T_1^{-1}C_6T_1T_2^{-1}C_6^{-1} = T_2^{-1}C_6T_1C_6^{-1} \\ &= C_6^6 = T_1^{-1}\sigma T_1\sigma^{-1} = T_2^{-1}\sigma T_1T_2^{-1}\sigma^{-1} \\ &= \sigma^2 = \sigma C_6\sigma C_6 = \mathbf{1}. \end{aligned} \quad (\text{B1})$$

We will assume the IGG is \mathbb{Z}_2 (see Sec. III), and assume the generator of the IGG is

$$b_{j\alpha} \rightarrow -b_{j\alpha}, \quad \alpha = \uparrow, \downarrow, \quad \forall j. \quad (\text{B2})$$

Elements of the IGG obviously preserves all mean field ansatz; therefore, the classification of algebraic spin liquid states are determined up to an IGG element.

For each space group element \mathcal{O} , we associate a U(1) phase $\mathcal{G}_{\mathcal{O}(i)}^{\mathcal{O}} = e^{i\phi_{\mathcal{O}}[\mathcal{O}(i)]}$ such that the mean field Hamiltonian is invariant under the combined PSG operation,

$$b_i \rightarrow \mathcal{G}_{\mathcal{O}(i)}^{\mathcal{O}} \mathcal{U}_{\mathcal{O}} b_{\mathcal{O}(i)}. \quad (\text{B3})$$

The \mathcal{U} matrices accounts for the effects of SOC (see their definitions in Sec. III).

Before solving for the PSG, we consider the effect of a pure gauge transformation $\mathcal{G} : b_{i\alpha} \rightarrow e^{i\phi_{\mathcal{G}}(i)} b_{i\alpha}$ on the U(1) phases $\mathcal{G}^{\mathcal{O}}$ associated to each group element. The symmetry operation on the gauge transformed boson reads $\mathcal{G}\mathcal{G}^{\mathcal{O}}\mathcal{U}_{\mathcal{O}}\mathcal{O}\mathcal{G}^{-1} = \mathcal{G}\mathcal{G}^{\mathcal{O}}\mathcal{U}_{\mathcal{O}}\mathcal{O}\mathcal{G}^{-1}\mathcal{O}^{-1}\mathcal{O}$. Since $\mathcal{U}_{\mathcal{O}}$ commutes with \mathcal{G} , $\mathcal{G}^{\mathcal{O}}$, and \mathcal{O} , $\mathcal{U}_{\mathcal{O}}$ cancel on both sides. Therefore $\mathcal{G}^{\mathcal{O}}$ should be replaced by $\mathcal{G}\mathcal{G}^{\mathcal{O}}\mathcal{O}\mathcal{G}^{-1}\mathcal{O}^{-1}$, or⁴¹

$$\phi_{\mathcal{O}}(i) \rightarrow \phi_{\mathcal{G}}(i) + \phi_{\mathcal{O}}(i) - \phi_{\mathcal{G}}(\mathcal{O}^{-1}(i)). \quad (\text{B4})$$

Using the gauge freedom one can always assume (open boundary condition)

$$\phi_{T_1}(x, y, w) = 0, \quad \phi_{T_2}(x = 0, y, w) = 0. \quad (\text{B5})$$

For the honeycomb lattice, this can be achieved by solving equations

$$\phi_{\mathcal{G}}(x, y, w) - \phi_{\mathcal{G}}(x - 1, y, w) + \phi_{T_1}(x, y, w) = 0, \quad (\text{B6})$$

$$\phi_{\mathcal{G}}(0, y, w) - \phi_{\mathcal{G}}(0, y - 1, w) + \phi_{T_2}(0, y, w) = 0. \quad (\text{B7})$$

For simplicity of notations we define $\Delta_1 f(x, y) = f(x + 1, y) - f(x, y)$ and $\Delta_2 f(x, y) = f(x, y + 1) - f(x, y)$.

The identity $T_1^{-1}T_2T_1T_2^{-1} = \mathbf{1}$ translates into the following equation of PSG elements,

$$(\mathcal{G}^{T_1}\mathcal{U}_{T_1}T_1)^{-1}(\mathcal{G}^{T_2}\mathcal{U}_{T_2}T_2)(\mathcal{G}^{T_1}\mathcal{U}_{T_1}T_1)(\mathcal{G}^{T_2}\mathcal{U}_{T_2}T_2)^{-1} = \pm \mathbf{1}, \quad (\text{B8})$$

where the RHS is an element of the IGG. In terms of phases,

$$\begin{aligned} -\phi_{T_1}[T_1(\mathbf{r})] + \phi_{T_2}[T_1(\mathbf{r})] + \phi_{T_1}[T_1T_2^{-1}(\mathbf{r})] - \phi_{T_2}[\mathbf{r}] \\ = \Delta_1\phi_{T_2}(x, y, w) \\ = p_1\pi, \end{aligned} \quad (\text{B9})$$

where $\mathbf{r} = (x, y, w)$, $p_1 \in \mathbb{Z}_2$, and we have adopted assumption in Eq. (B5). Again from Eq. (B5), we see that

$$\phi_{T_2}(x, y, w) = p_1\pi x. \quad (\text{B10})$$

In other words, the flux in one elementary hexagon is $p_1\pi$.

Similarly, from $T_1^{-1}C_6T_1T_2^{-1}C_6^{-1} = T_2^{-1}C_6T_1C_6^{-1} = \mathbf{1}$ we have

$$(\mathcal{G}^{T_1}\mathcal{U}_{T_1}T_1)^{-1}(\mathcal{G}^{C_6}\mathcal{U}_{C_6}C_6)(\mathcal{G}^{T_1}\mathcal{U}_{T_1}T_1) \\ (\mathcal{G}^{T_2}\mathcal{U}_{T_2}T_2)^{-1}(\mathcal{G}^{C_6}\mathcal{U}_{C_6}C_6)^{-1} = \pm \mathbf{1}, \quad (\text{B11})$$

$$(\mathcal{G}^{T_2}\mathcal{U}_{T_2}T_2)^{-1}(\mathcal{G}^{C_6}\mathcal{U}_{C_6}C_6) \\ (\mathcal{G}^{T_1}\mathcal{U}_{T_1}T_1)(\mathcal{G}^{C_6}\mathcal{U}_{C_6}C_6)^{-1} = \pm \mathbf{1}. \quad (\text{B12})$$

The $\mathcal{U}_{\mathcal{O}}$'s cancel, and the solution for the U(1) phases is

$$\Delta_1\phi_{C_6}(x, y, w) = p_1\pi(x + y) + p_2\pi, \quad (\text{B13})$$

$$\Delta_2\phi_{C_6}(x, y, w) = p_1\pi x + p_3\pi. \quad (\text{B14})$$

Performing pure gauge transformations, we may further assume⁴²

$$p_2 = p_3 = 0, \quad \phi_{C_6}(0, 0, u) = \phi_{C_6}(0, 0, v). \quad (\text{B15})$$

The solution for ϕ_{C_6} reads

$$\begin{aligned} \phi_{C_6}(x, y, w) &= \phi_{C_6}(0, 0, w) \\ &+ p_1\pi \frac{x(x + 2y - 1)}{2}. \end{aligned} \quad (\text{B16})$$

In the PSG formulation of the group relation $T_1^{-1}\sigma T_1\sigma^{-1} = T_2^{-1}\sigma T_1T_2^{-1}\sigma^{-1} = \mathbf{1}$, the \mathcal{U}_{σ} 's again cancel. Thus we have

$$\Delta_1\phi_{\sigma}(x, y, w) = p_4\pi, \quad (\text{B17})$$

$$\Delta_2\phi_{\sigma}(x, y, w) = p_1\pi y + p_5\pi. \quad (\text{B18})$$

The solution for ϕ_{σ} is

$$\begin{aligned} \phi_{\sigma}(x, y, w) &= \phi_{\sigma}(0, 0, w) + \frac{1}{2}p_1\pi y(y - 1) \\ &+ p_4\pi x + p_5\pi y. \end{aligned} \quad (\text{B19})$$

From $C_6^6 = \mathbf{1}$ we have

$$(\mathcal{G}^{C_6}\mathcal{U}_{C_6}C_6)^6 = (\mathcal{U}_{C_6})^6(\mathcal{G}^{C_6}C_6)^6 = \pm \mathbf{1}, \quad (\text{B20})$$

since \mathcal{U}_{C_6} acts only on the spin indices and commutes with \mathcal{G}^{C_6} and C_6 . Since $(\mathcal{U}_{C_6})^6 = -\mathbf{1}$, the above equation simplifies to $(\mathcal{G}^{C_6}C_6)^6 = \pm \mathbf{1}$, giving

$$\begin{aligned} 3[\phi_{C_6}(0, 0, u) + \phi_{C_6}(0, 0, v)] \\ = (p_1 + p_2)\pi + p_6\pi. \end{aligned} \quad (\text{B21})$$

Bond	$(x, y, u)-(x, y, v)$	$(x, y, u)-(x+1, y-1, v)$	$(x, y, u)-(x, y-1, v)$
$u_{\uparrow\uparrow}^A$	u_s^A	$(-)^{p_1(y+1)}u_s^A$	u_s^A
$u_{\downarrow\downarrow}^A$	$(-)^{p_9}u_s^A$	$(-)^{p_1(y+1)+p_9}u_s^A$	$(-)^{p_9}u_s^A$
$u_{\uparrow\downarrow}^A$	$e^{i(p_9/2)\pi}u_a^A$	$e^{i(p_9/2+2/3+p_1(y+1))\pi}u_a^A$	$e^{i(p_9/2-2/3)\pi}u_a^A$
$u_{\downarrow\uparrow}^A$	$-e^{-i(p_9/2)\pi}u_a^A$	$-e^{-i(p_9/2+2/3+p_1(y+1))\pi}u_a^A$	$-e^{-i(p_9/2-2/3)\pi}u_a^A$
$u_{\uparrow\uparrow}^B$	u_s^B	$e^{i(-2/3+p_1(y+1))\pi}u_s^B$	$e^{i(+2/3)\pi}u_s^B$
$u_{\downarrow\downarrow}^B$	$(-1)^{1+p_7}u_s^B$	$(-1)^{1+p_7}e^{i(+2/3+p_1(y+1))\pi}u_s^B$	$(-1)^{1+p_7}e^{i(-2/3)\pi}u_s^B$
$u_{\uparrow\downarrow}^B$	u_a^B	$(-)^{p_1(y+1)}u_a^B$	u_a^B
$u_{\downarrow\uparrow}^B$	$(-)^{p_7+p_8+p_9}u_a^B$	$(-)^{p_7+p_8+p_9+p_1(y+1)}u_a^B$	$(-)^{p_7+p_8+p_9}u_a^B$
Bond	$(x, y, v)-(x, y, u)$	$(x, y, v)-(x, y+1, u)$	$(x, y, v)-(x-1, y+1, u)$
$u_{\uparrow\uparrow}^A$	u_s^A	u_s^A	$(-)^{p_1y}u_s^A$
$u_{\downarrow\downarrow}^A$	$(-)^{p_9}u_s^A$	$(-)^{p_9}u_s^A$	$(-)^{p_1y+p_9}u_s^A$
$u_{\uparrow\downarrow}^A$	$-e^{i(p_9/2)\pi}u_a^A$	$-e^{i(p_9/2-2/3)\pi}u_a^A$	$-e^{i(p_9/2+2/3+p_1y)\pi}u_a^A$
$u_{\downarrow\uparrow}^A$	$e^{-i(p_9/2)\pi}u_a^A$	$e^{-i(p_9/2-2/3)\pi}u_a^A$	$e^{-i(p_9/2+2/3+p_1y)\pi}u_a^A$
$u_{\uparrow\uparrow}^B$	u_s^B	$e^{i(+2/3)\pi}u_s^B$	$e^{i(-2/3+p_1y)\pi}u_s^B$
$u_{\downarrow\downarrow}^B$	$(-1)^{1+p_7}u_s^B$	$(-1)^{1+p_7}e^{i(-2/3)\pi}u_s^B$	$(-1)^{1+p_7}e^{i(+2/3+p_1y)\pi}u_s^B$
$u_{\uparrow\downarrow}^B$	$(-)^{p_7+p_8+p_9}u_a^B$	$(-)^{p_7+p_8+p_9}u_a^B$	$(-)^{p_7+p_8+p_9+p_1y}u_a^B$
$u_{\downarrow\uparrow}^B$	u_a^B	u_a^B	$(-)^{p_1y}u_a^B$

TABLE III. Spatial patterns of the nearest-neighbor mean-field ansatz. u_s^A, u_a^A, u_s^B and u_a^B are real numbers. The coefficients are subject to constraints from hermiticity and time reversal symmetry.

For $\sigma^2 = \mathbf{1}$ we have

$$(\mathcal{G}^\sigma \mathcal{U}_\sigma \sigma)^2 = (\mathcal{U}_\sigma)^2 (\mathcal{G}^\sigma \sigma)^2 = -(\mathcal{G}^\sigma \sigma)^2 = \pm \mathbf{1}, \quad (\text{B22})$$

where \mathcal{U}_σ commutes with the rest, and $(\mathcal{U}_\sigma)^2 = -\mathbf{1}$. This results in the constraint

$$\phi_\sigma(0, 0, u) + \phi_\sigma(0, 0, v) = (p_1 y^2 + p_4 y + p_7) \pi. \quad (\text{B23})$$

We see immediately $p_1 = p_4$ by comparing $y = 0$ and $y = 1$ in this equation.

From $\sigma C_6 \sigma C_6$ we have

$$\begin{aligned} & (\mathcal{G}^\sigma \mathcal{U}_\sigma \sigma) (\mathcal{G}^{C_6} \mathcal{U}_{C_6} C_6) (\mathcal{G}^\sigma \mathcal{U}_\sigma \sigma) (\mathcal{G}^{C_6} \mathcal{U}_{C_6} C_6) \\ &= (\mathcal{U}_\sigma \mathcal{U}_{C_6} \mathcal{U}_\sigma \mathcal{U}_{C_6}) (\mathcal{G}^\sigma \sigma) (\mathcal{G}^{C_6} C_6) (\mathcal{G}^\sigma \sigma) (\mathcal{G}^{C_6} C_6) \\ &= -(\mathcal{G}^\sigma \sigma) (\mathcal{G}^{C_6} C_6) (\mathcal{G}^\sigma \sigma) (\mathcal{G}^{C_6} C_6) \\ &= \pm \mathbf{1}. \end{aligned} \quad (\text{B24})$$

Therefore we have

$$2\phi_\sigma(0, 0, v) + 2\phi_{C_6}(0, 0, u) = 2\phi_\sigma(0, 0, u) + 2\phi_{C_6}(0, 0, v) = p_8 \pi. \quad (\text{B25})$$

and $p_1 = p_5$. Due to Eq. (B15), we see that $2\phi_\sigma(0, 0, v) = 2\phi_\sigma(0, 0, u)$, giving

$$\phi_\sigma(0, 0, u) - \phi_\sigma(0, 0, v) = p_9 \pi. \quad (\text{B26})$$

$\phi_{C_6}(0, 0, w)$ and $\phi_\sigma(0, 0, w)$ can be solved,

$$\phi_\sigma(0, 0, u) = (p_7 + p_9) \pi / 2 \bmod 2\pi, \quad (\text{B27})$$

$$\phi_\sigma(0, 0, v) = (p_7 - p_9) \pi / 2 \bmod 2\pi, \quad (\text{B28})$$

$$\phi_{C_6}(0, 0, w) = (p_7 + p_8 + p_9) \pi / 2 \bmod 2\pi, \quad (\text{B29})$$

and $p_6 = p_1 + p_7 + p_8 + p_9$ from Eq. (B21).

Summarizing, the solutions of the PSG are

$$\phi_{T_1}(x, y, w) = 0, \quad (\text{B30})$$

$$\phi_{T_2}(x, y, w) = p_1 \pi x, \quad (\text{B31})$$

$$\phi_{C_6}(x, y, w) = \frac{\pi}{2} [p_1 x(x + 2y - 1) + p_7 + p_8 + p_9], \quad (\text{B32})$$

$$\phi_\sigma(x, y, u) = \frac{\pi}{2} [2p_1 x + p_1 y(y + 1) + p_7 + p_9], \quad (\text{B33})$$

$$\phi_\sigma(x, y, v) = \frac{\pi}{2} [2p_1 x + p_1 y(y + 1) + p_7 - p_9]. \quad (\text{B34})$$

where $w = u, v$ and p_1, p_7, p_8, p_9 are free to take either 0 or 1 in \mathbb{Z}_2 . There are in total 16 possible classes of QSLs; the mean field ansatz would further constrain the number of free parameters. The respective gauge transformations for the 16 \mathbb{Z}_2 QSLs are summarized in Tab. I.

Appendix C: Nearest neighbor mean field ansatz of the \mathbb{Z}_2 PSG

In this appendix we present symmetry allowed mean field ansatz up to nearest neighbors.

The algebraic solution of PSG is very general and usually contains many free parameters. Certain mean field ansatz will put further constraints on the PSG. In particular, if a non-identity space group element \mathcal{O} transforms a bond to itself or its inverse, the form of exchange terms on this bond will be constrained.

We first consider the spin-flipping pairing terms (u_a^B terms). Under the action of σ ,

$$u_a^B b_{(0,0,u)\uparrow} b_{(0,0,v)\downarrow} \rightarrow e^{i(p_7+1)\pi} u_a^B b_{(0,0,u)\uparrow} b_{(0,0,v)\downarrow}. \quad (\text{C1})$$

Therefore nonzero u_a^B requires $p_7 = 1$. Under $T_1^{-1}C_6^3$,

$$u_a^B b_{(0,0,u)\uparrow} b_{(0,0,v)\downarrow} \rightarrow e^{i(p_7+p_8+p_9)\pi} u_a^B b_{(0,0,u)\downarrow} b_{(0,0,v)\uparrow}. \quad (\text{C2})$$

This equation requires $u_a^B = e^{i(p_7+p_8+p_9)} u_a^B$.

Similarly we define $u_s^{A\uparrow} = u_{(0,0,u),(0,0,v),\uparrow\uparrow}^A$ and $u_s^{A\downarrow} = u_{(0,0,u),(0,0,v),\downarrow\downarrow}^A$. Acting σ and $T_1^{-1}C_6^3$ on the S term,

$$\sigma : u_s^{A\uparrow} b_{(0,0,u)\uparrow}^\dagger b_{(0,0,v)\uparrow} \rightarrow e^{ip_9\pi} u_s^{A\uparrow} b_{(0,0,u)\downarrow}^\dagger b_{(0,0,u)\downarrow}, \quad (\text{C3})$$

$$T_1^{-1}C_6^3 : u_s^{A\uparrow} b_{(0,0,u)\uparrow}^\dagger b_{(0,0,v)\uparrow} \rightarrow u_s^{A\uparrow} b_{(0,0,v)\uparrow}^\dagger b_{(0,0,u)\uparrow}. \quad (\text{C4})$$

From Eq. (C4) we immediately conclude that if we require $u_s^{A\uparrow} \neq 0$, then $u_s^{A\uparrow} = u_s^{A\uparrow*}$, $u_s^{A\downarrow} = u_s^{A\downarrow*}$, and $u_s^{A\uparrow} = u_s^{A\downarrow} e^{ip_9\pi}$.

Applying σ and $T_1^{-1}C_6^3$ on the $u_s^{B\uparrow} = u_{(0,0,u),(0,0,v),\uparrow\uparrow}^B$ term, we see that

$$\sigma : u_s^{B\uparrow} b_{(0,0,u)\uparrow} b_{(0,0,v)\uparrow} \rightarrow e^{i(p_7+1)\pi} u_s^{B\uparrow} b_{(0,0,u)\downarrow} b_{(0,0,v)\downarrow}, \quad (\text{C5})$$

$$T_1^{-1}C_6^3 : u_s^{B\uparrow} b_{(0,0,u)\uparrow} b_{(0,0,v)\uparrow} \rightarrow e^{i(p_7+p_8+p_9+1)\pi} u_s^{B\uparrow} b_{(0,0,u)\uparrow} b_{(0,0,v)\uparrow}. \quad (\text{C6})$$

and similarly for $u_s^{B\downarrow}$. It is obvious that such terms are nonzero only when $p_7 + p_8 + p_9 = 1$.

Following the same procedures, we find for u_a^A terms

$$u_{(0,0,u),(0,0,v),\uparrow\downarrow}^{A*} = u_{(0,0,u),(0,0,v),\uparrow\downarrow}^A e^{ip_9\pi}, \quad (\text{C7})$$

$$u_{(0,0,u),(0,0,v),\uparrow\downarrow}^A = -u_{(0,0,v),(0,0,u),\uparrow\downarrow}^A, \quad (\text{C8})$$

and similarly for $u_{(0,0,u),(0,0,v),\downarrow\uparrow}^A$ and $u_{(0,0,v),(0,0,u),\downarrow\uparrow}^A$.

We construct exchange interactions on all lattice bonds by applying symmetry operations. The results are shown in Tab. III.

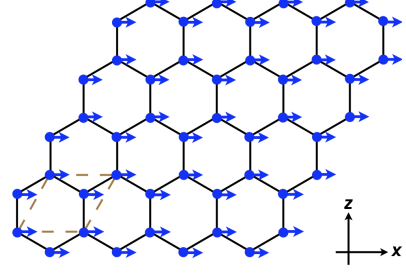


FIG. 5. The typical magnetic ordering structure for a \mathbb{Z}_2A100 state. The order is ferromagnetic, but the direction depends on the details of the condensate. The gray dashed lines denote the unit cell. The parameters of the Hamiltonian are the same as in Fig. 3.

Appendix D: Fractionalization of crystal momentum and enhanced periodicity

Defining $\mathcal{O}^s = \mathcal{G}\mathcal{U}_\mathcal{O}\mathcal{O}$ to be the symmetry group element acting on the spinon sector, we know from previous discussions that

$$T_1 \hat{T}_2 \hat{T}_1^{-1} \hat{T}_2^{-1} = (-1)^{p_1}. \quad (\text{D1})$$

Given a two-spinon product state $|a\rangle = |\mathbf{q}_a, \Omega_a\rangle$ with total momentum \mathbf{q}_a and total energy Ω_a , the translation operator acts on it by

$$\hat{T}_\mu |a\rangle = \hat{T}_\mu(1) \hat{T}_\mu(2) |a\rangle = e^{iq_a^\mu} |a\rangle \quad (\text{D2})$$

where $q_a^\mu = \mathbf{q} \cdot \mathbf{a}_\mu$. We can construct another three states by translating the second spinon

$$|b\rangle = \hat{T}_1(2) |a\rangle, \quad (\text{D3})$$

$$|c\rangle = \hat{T}_2(2) |a\rangle, \quad (\text{D4})$$

$$|d\rangle = \hat{T}_1(2) \hat{T}_2(2) |a\rangle. \quad (\text{D5})$$

These states have the same energy as $|a\rangle$, but with translated momenta,

$$(q_b^1, q_b^2) = (q_a^1, q_a^2 + p_1\pi), \quad (\text{D6})$$

$$(q_c^1, q_c^2) = (q_a^1 + p_1\pi, q_a^2), \quad (\text{D7})$$

$$(q_d^1, q_d^2) = (q_a^1 + p_1\pi, q_a^2 + p_1\pi). \quad (\text{D8})$$

Therefore, the two-spinon spectrum has an enhanced periodicity if $p_1 = 1$. In particular, the lower edge of $\mathcal{S}(\mathbf{q}, \omega)$

$$\text{edge}(\mathbf{q}) = \min_{\mathbf{k}} [\omega(\mathbf{k}) + \omega(\mathbf{q} - \mathbf{k})] \quad (\text{D9})$$

is completely encoded in energies of the two-spinons states with the momentum \mathbf{q} , thus has the same periodicity,

$$\begin{aligned} \text{edge}(\mathbf{q}_a) &= \text{edge}(\mathbf{q}_b) \\ &= \text{edge}(\mathbf{q}_c) = \text{edge}(\mathbf{q}_d). \end{aligned} \quad (\text{D10})$$

Otherwise $p_1 = 0$, and the lower excitation edge should have the usual periodicity of 2π in both directions of Brillouin zone basis.

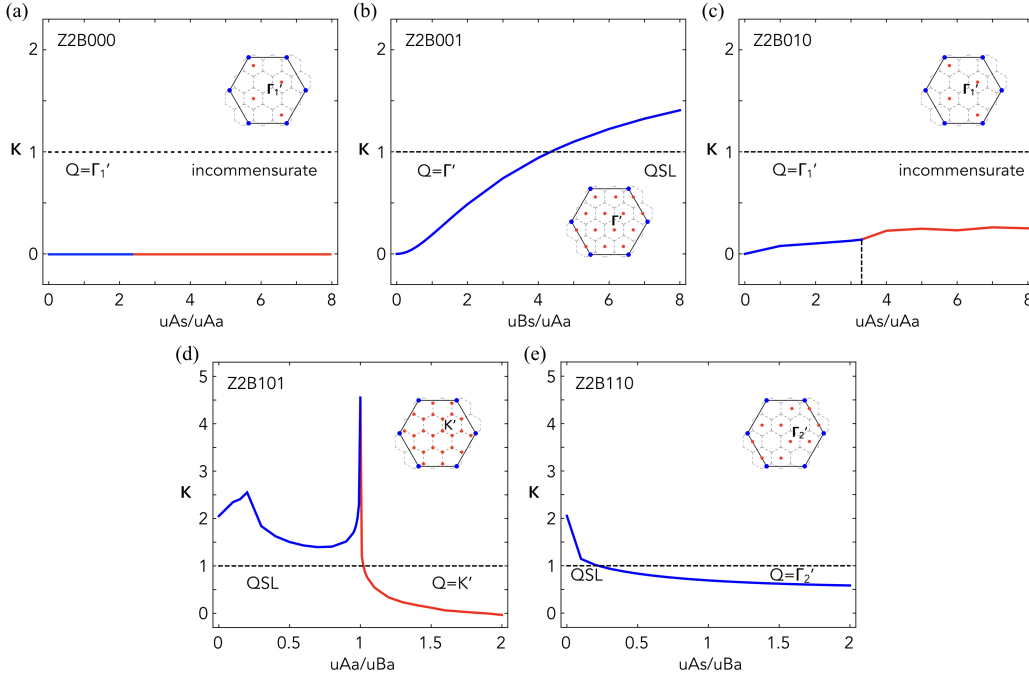


FIG. 6. (Color online.) The phase diagrams for all other mean-field Hamiltonians in the $\mathbb{Z}2\mathbb{B}$ class. The nonzero parameters are listed in Tab. II. We choose $u_s^B/u_s^A = 0.6$ in (c), and $u_a^A/u_s^A = 0.6$ in (e).

We have shown that commuting and anticommuting single spinon translations gives different spectroscopic features. We now consider presentations of the symmetry group involving translations (since we are ultimately interested in the periodicity in the reciprocal space) on one-spinon sector,

$$\hat{T}_1^{-1} \hat{C}_6 \hat{T}_1 \hat{T}_2^{-1} \hat{C}_6^{-1} = (-1)^{p_2}, \quad (\text{D11})$$

$$\hat{T}_2^{-1} \hat{C}_6 \hat{T}_1 \hat{C}_6^{-1} = (-1)^{p_3}, \quad (\text{D12})$$

$$\hat{T}_1^{-1} \hat{\sigma} \hat{T}_1 \hat{\sigma}^{-1} = (-1)^{p_4}, \quad (\text{D13})$$

$$\hat{T}_2^{-1} \hat{\sigma} \hat{T}_1 \hat{T}_2^{-1} \hat{\sigma}^{-1} = (-1)^{p_5}. \quad (\text{D14})$$

where we followed the convention in Appendix A. Due to the gauge freedom, we can fix p_2 and p_3 to be 0, and consistency of the PSG solution requires $p_4 = p_5 = p_1$. With a detailed analysis, we found that Eq. (D11), Eq. (D12) and Eq. (D14) do not give to any obvious type of periodicity, while Eq. (D13) gives a fuzzier version of the one constructed by considering translations only. Therefore, considering the whole symmetry group does not introduce more detailed implications of the neutron scattering spectrum.

Rewriting Eq. (D11)–(D14) in a more convenient form, and taking $p_2 = p_3 = 0$, $p_4 = p_5 = p_1$, we get

$$\hat{T}_1 \hat{C}_6 = \hat{C}_6 \hat{T}_1 \hat{T}_2^{-1}, \quad (\text{D15})$$

$$\hat{T}_2 \hat{C}_6 = \hat{C}_6 \hat{T}_1, \quad (\text{D16})$$

$$\hat{T}_1 \hat{\sigma} = (-1)^{p_1} \hat{\sigma} \hat{T}_1, \quad (\text{D17})$$

$$\hat{T}_2 \hat{\sigma} = (-1)^{p_1} \hat{\sigma} \hat{T}_1 \hat{T}_2^{-1}. \quad (\text{D18})$$

Suppose $|a\rangle = |\mathbf{q}_a, \Omega_a\rangle$ is a two-spinon product state, we try acting \hat{C}_6 on the second spinon to obtain new eigenstates $|b\rangle = \hat{C}_6(2)|a\rangle$ with the same energy. Then

$$\begin{aligned} T_1|b\rangle &= \hat{T}_1(1) \hat{T}_1(2) \hat{C}_6(2)|a\rangle \\ &= \hat{C}_6(2) \hat{T}_1(1) \hat{T}_1(2) \hat{T}_2^{-1}(2)|a\rangle \\ &= e^{i(q_a^1 - k^2(2))} |b\rangle, \end{aligned} \quad (\text{D19})$$

$$\begin{aligned} T_2|b\rangle &= T_2^s(1) T_2^s(2) \hat{C}_6(2)|a\rangle \\ &= \hat{C}_6(2) T_2^s(1) \hat{T}_1(2)|a\rangle \\ &= e^{i(k^2(1) + k^1(2))} |b\rangle, \end{aligned} \quad (\text{D20})$$

where $\mathbf{k}(i)$ are the momenta for individual spinons. The result depends on the single spinon momentum, and does not lead to any obvious extra periodicity.

Similarly, let $|c\rangle = \hat{\sigma}(2)|a\rangle$,

$$\begin{aligned} T_1|c\rangle &= \hat{T}_1(1) \hat{T}_1(2) \hat{\sigma}(2)|a\rangle \\ &= (-1)^{p_1} \hat{\sigma}(2) \hat{T}_1(1) \hat{T}_1(2)|a\rangle \\ &= (-1)^{p_1} e^{iq_a^1} |c\rangle, \end{aligned} \quad (\text{D21})$$

$$\begin{aligned} T_2|c\rangle &= T_2^s(1) T_2^s(2) \hat{\sigma}(2)|a\rangle \\ &= (-1)^{p_1} \hat{\sigma}(2) T_2^s(1) \hat{T}_1(2) \hat{T}_2^{-1}(2)|a\rangle \\ &= (-1)^{p_1} e^{i(k^2(1) + k^1(2) - k^2(2))} |c\rangle. \end{aligned} \quad (\text{D22})$$

While the second equation does not tell us much, the first one does carries (q_a^1, q_a^2) to (q_c^1, q_c^2) with $q_c^1 = q_a^1 + p_1\pi$, while we cannot say much about q_c^2 and q_a^2 . This is a fuzzier version of Eq. (D10) as it does not carry as much information about the structure of the spectrum.

Appendix E: Proximate magnetic order of \mathbb{Z}_2 QSLs

1. $\mathbb{Z}_2\text{A}$ states

Here we briefly comment on the proximate magnetic order resulting from the $\mathbb{Z}_2\text{A}$ parent state. In this case, the translation symmetry is not fractionalized, and the proximate magnetic order also preserves such a symmetry. For a large range of parameters, the band minimum is at $\Gamma = (0, 0)$, giving rise to a ferromagnetic order. The ordering pattern for a typical set of parameters is shown in Fig. 5.

2. $\mathbb{Z}_2\text{B}$ states

In this section we discuss other $\mathbb{Z}_2\text{B}$ mean field classes in the PSG classification. Among them the $\mathbb{Z}_2\text{B011}$ class has only one nonzero parameter u_a^A , and the corresponding ground state is magnetically ordered with ordering wave vector Γ'_1 and Γ'_2 . Phase diagrams of the other classes are shown in Fig. 6.

We see that for the parameter space we choose, the $\mathbb{Z}_2\text{B000}$ and $\mathbb{Z}_2\text{B010}$ states are always ordered, while $\mathbb{Z}_2\text{B001}$, $\mathbb{Z}_2\text{B101}$, and $\mathbb{Z}_2\text{B110}$ can all support a QSL phase. The ordering wave vector Γ'_1 for $\mathbb{Z}_2\text{B000}$ and $\mathbb{Z}_2\text{B010}$ are the same as that of the $\mathbb{Z}_2\text{B100}$ described and discussed in Sec. III and Sec. IV, and thus consistent with the magnetic Bragg peak at $(\pi, 0)$.

-
- * Currently on leave from Fudan University, China; gangchen.physics@gmail.com
- ¹ A. Kitaev, *Annals of Physics* **321**, 2 (2006).
 - ² G. Jackeli and G. Khaliullin, *Phys. Rev. Lett.* **102**, 017205 (2009).
 - ³ K. Kitagawa, T. Takayama, Y. Matsumoto, A. Kato, R. Takano, Y. Kishimoto, S. Bette, R. Dinnebier, G. Jackeli, and H. Takagi, *Nature* **554**, 341 (2018).
 - ⁴ J. Terzic, J. C. Wang, F. Ye, W. H. Song, S. J. Yuan, S. Aswartham, L. E. DeLong, S. V. Streltsov, D. I. Khomskii, and G. Cao, *Phys. Rev. B* **91**, 235147 (2015).
 - ⁵ R. Comin, G. Levy, B. Ludbrook, Z.-H. Zhu, C. N. Veenstra, J. A. Rosen, Y. Singh, P. Gegenwart, D. Stricker, J. N. Hancock, D. van der Marel, I. S. Elfimov, and A. Damascelli, *Phys. Rev. Lett.* **109**, 266406 (2012).
 - ⁶ C. H. Sohn, H.-S. Kim, T. F. Qi, D. W. Jeong, H. J. Park, H. K. Yoo, H. H. Kim, J.-Y. Kim, T. D. Kang, D.-Y. Cho, G. Cao, J. Yu, S. J. Moon, and T. W. Noh, *Phys. Rev. B* **88**, 085125 (2013).
 - ⁷ F. Ye, S. Chi, H. Cao, B. C. Chakoumakos, J. A. Fernandez-Baca, R. Custelcean, T. F. Qi, O. B. Korneta, and G. Cao, *Phys. Rev. B* **85**, 180403 (2012).
 - ⁸ H. Gretarsson, J. P. Clancy, Y. Singh, P. Gegenwart, J. P. Hill, J. Kim, M. H. Upton, A. H. Said, D. Casa, T. Gog, and Y.-J. Kim, *Phys. Rev. B* **87**, 220407 (2013).
 - ⁹ H. Gretarsson, J. P. Clancy, X. Liu, J. P. Hill, E. Bozin, Y. Singh, S. Manni, P. Gegenwart, J. Kim, A. H. Said, D. Casa, T. Gog, M. H. Upton, H.-S. Kim, J. Yu, V. M. Katukuri, L. Hozoi, J. van den Brink, and Y.-J. Kim, *Phys. Rev. Lett.* **110**, 076402 (2013).
 - ¹⁰ X. Liu, T. Berlijn, W.-G. Yin, W. Ku, A. Tsvelik, Y.-J. Kim, H. Gretarsson, Y. Singh, P. Gegenwart, and J. P. Hill, *Phys. Rev. B* **83**, 220403 (2011).
 - ¹¹ T. Takayama, A. Kato, R. Dinnebier, J. Nuss, H. Kono, L. S. I. Veiga, G. Fabbri, D. Haskel, and H. Takagi, *Phys. Rev. Lett.* **114**, 077202 (2015).
 - ¹² K. A. Modic, T. E. Smidt, I. Kimchi, N. P. Breznay, A. Biffin, S. Choi, R. D. Johnson, R. Coldea, P. Watkins-Curry, G. T. McCandless, J. Y. Chan, F. Gandara, Z. Islam, A. Vishwanath, A. Shekhter, R. D. McDonald, and J. G. Analytis, *Nature Communications* **5**, 4203 (2014).
 - ¹³ L. Binotto, I. Pollini, and G. Spinolo, *Physica Status Solidi (b)* **44**, 245 (1971).
 - ¹⁴ I. Pollini, *Phys. Rev. B* **53**, 12769 (1996).
 - ¹⁵ K. W. Plumb, J. P. Clancy, L. J. Sandilands, V. V. Shankar, Y. F. Hu, K. S. Burch, H.-Y. Kee, and Y.-J. Kim, *Phys. Rev. B* **90**, 041112 (2014).
 - ¹⁶ L. J. Sandilands, Y. Tian, A. A. Reijnders, H.-S. Kim, K. W. Plumb, Y.-J. Kim, H.-Y. Kee, and K. S. Burch, *Phys. Rev. B* **93**, 075144 (2016).
 - ¹⁷ A. Banerjee, C. Bridges, J.-Q. Yan, A. Aczel, L. Li, M. Stone, G. Granroth, M. Lumsden, Y. Yiu, J. Knolle, *et al.*, *Nature materials* **15**, 733740 (2016).
 - ¹⁸ A. Banerjee, J. Yan, J. Knolle, C. A. Bridges, M. B. Stone, M. D. Lumsden, D. G. Mandrus, D. A. Tennant, R. Moessner, and S. E. Nagler, *Science* **356**, 1055 (2017).
 - ¹⁹ Y. Okamoto, M. Nohara, H. Aruga-Katori, and H. Takagi, *Phys. Rev. Lett.* **99**, 137207 (2007).
 - ²⁰ B. J. Kim, H. Jin, S. J. Moon, J.-Y. Kim, B.-G. Park, C. S. Leem, J. Yu, T. W. Noh, C. Kim, S.-J. Oh, J.-H. Park, V. Durairaj, G. Cao, and E. Rotenberg, *Phys. Rev. Lett.* **101**, 076402 (2008).
 - ²¹ G. Chen and L. Balents, *Phys. Rev. B* **78**, 094403 (2008).
 - ²² S. Trebst, arXiv:1701.07056 (2017).
 - ²³ Y. Zhou, K. Kanoda, and T.-K. Ng, *Rev. Mod. Phys.* **89**, 025003 (2017).
 - ²⁴ J. Knolle and R. Moessner, 1804.02037 (2018).
 - ²⁵ M. Hermanns, I. Kimchi, and J. Knolle, *Annual Review of Condensed Matter Physics* **9**, 17 (2018).
 - ²⁶ L. Savary and L. Balents, *Rep. Prog. Phys.* **80**, 016502 (2017).
 - ²⁷ F.-Y. Li, Y.-D. Li, Y. Yu, A. Paramekanti, and G. Chen, *Phys. Rev. B* **95**, 085132 (2017).
 - ²⁸ J. G. Rau and M. J. P. Gingras, *Phys. Rev. B* **98**, 054408 (2018).
 - ²⁹ S.-H. Jang, R. Sano, Y. Kato, and Y. Motome, arXiv:1807.01443 (2018).
 - ³⁰ J. G. Rau, E. K.-H. Lee, and H.-Y. Kee, *Phys. Rev. Lett.* **112**, 077204 (2014).
 - ³¹ H.-C. Jiang, Z.-C. Gu, X.-L. Qi, and S. Trebst, *Phys. Rev. B* **83**, 245104 (2011).
 - ³² J. c. v. Chaloupka, G. Jackeli, and G. Khaliullin, *Phys. Rev. Lett.* **110**, 097204 (2013).
 - ³³ J. Nasu, Y. Kato, J. Yoshitake, Y. Kamiya, and Y. Motome, *Phys. Rev. Lett.* **118**, 137203 (2017).
 - ³⁴ I. Rousochatzakis, J. Reuther, R. Thomale, S. Rachel, and

- N. B. Perkins, *Phys. Rev. X* **5**, 041035 (2015).
- ³⁵ Y. Sizyuk, C. Price, P. Wölffe, and N. B. Perkins, *Phys. Rev. B* **90**, 155126 (2014).
- ³⁶ S.-S. Gong, D. N. Sheng, O. I. Motrunich, and M. P. A. Fisher, *Phys. Rev. B* **88**, 165138 (2013).
- ³⁷ Z. Wang, J. Guo, F. F. Tafti, A. Hegg, S. Sen, V. A. Sidorov, L. Wang, S. Cai, W. Yi, Y. Zhou, H. Wang, S. Zhang, K. Yang, A. Li, X. Li, Y. Li, J. Liu, Y. Shi, W. Ku, Q. Wu, R. J. Cava, and L. Sun, *Phys. Rev. B* **97**, 245149 (2018).
- ³⁸ N. Read and S. Sachdev, *Phys. Rev. Lett.* **66**, 1773 (1991).
- ³⁹ X.-G. Wen, *Physics Letters A* **300**, 175 (2002).
- ⁴⁰ X.-G. Wen, *Phys. Rev. B* **65**, 165113 (2002).
- ⁴¹ F. Wang and A. Vishwanath, *Phys. Rev. B* **74**, 174423 (2006).
- ⁴² F. Wang, *Phys. Rev. B* **82**, 024419 (2010).
- ⁴³ Y.-D. Li, Y.-M. Lu, and G. Chen, *Phys. Rev. B* **96**, 054445 (2017).
- ⁴⁴ J. Reuther, S.-P. Lee, and J. Alicea, *Phys. Rev. B* **90**, 174417 (2014).
- ⁴⁵ R. Schaffer, S. Bhattacharjee, and Y. B. Kim, *Phys. Rev. B* **88**, 174405 (2013).
- ⁴⁶ S. Sachdev, *Phys. Rev. B* **45**, 12377 (1992).
- ⁴⁷ J. A. Sears, M. Songvilay, K. W. Plumb, J. P. Clancy, Y. Qiu, Y. Zhao, D. Parshall, and Y.-J. Kim, *Phys. Rev. B* **91**, 144420 (2015).
- ⁴⁸ A. M. Essin and M. Hermele, *Phys. Rev. B* **87**, 104406 (2013).
- ⁴⁹ A. M. Essin and M. Hermele, *Phys. Rev. B* **90**, 121102 (2014).
- ⁵⁰ Y. Kasahara, K. Sugii, T. Ohnishi, M. Shimozawa, M. Yamashita, N. Kurita, H. Tanaka, J. Nasu, Y. Motome, T. Shibauchi, and Y. Matsuda, *Phys. Rev. Lett.* **120**, 217205 (2018).
- ⁵¹ R. Hentrich, M. Roslova, A. Isaeva, T. Doert, W. Brenig, B. Büchner, and C. Hess, *Phys. Rev. B* **99**, 085136 (2019).
- ⁵² Y. Kasahara, T. Ohnishi, Y. Mizukami, O. Tanaka, S. Ma, K. Sugii, N. Kurita, H. Tanaka, J. Nasu, Y. Motome, T. Shibauchi, and Y. Matsuda, *Nature* **559**, 227231 (2018).
- ⁵³ M. Ye, G. B. Halász, L. Savary, and L. Balents, *Phys. Rev. Lett.* **121**, 147201 (2018).
- ⁵⁴ Y. Vinkler-Aviv and A. Rosch, *Phys. Rev. X* **8**, 031032 (2018).
- ⁵⁵ E. A. Ghioldi, M. G. Gonzalez, S.-S. Zhang, Y. Kamiya, L. O. Manuel, A. E. Trumper, and C. D. Batista, *Phys. Rev. B* **98**, 184403 (2018).
- ⁵⁶ Z.-X. Liu and B. Normand, *Phys. Rev. Lett.* **120**, 187201 (2018).
- ⁵⁷ C. Hickey and S. Trebst, *Nature Communications* **10**, 530 (2019).
- ⁵⁸ H.-C. Jiang, C.-Y. Wang, B. Huang, and Y.-M. Lu, arXiv:1809.08247 (2018).
- ⁵⁹ L. Zou and Y.-C. He, arXiv:1809.09091 (2018).